05

Spectra of optical harmonics 2 and 3/2 at subrelativistic laser-plasma generation of X-ray radiation

© M.V. Chaschin[1], P.A. Shcheglov[1], A.A. Tausenev[1,2], M.M. Nazarov[1], V.M. Gordienko[2]

[1] National Research Center „Kurchatov Institute“,
123182 Moscow, Russia
[2] Faculty of Physics, Lomonosov Moscow State University,
119234 Moscow, Russia

e-mail: chamike12@gmail.com

Received December 02, 2022
Revised January 16, 2023
Accepted January 28, 2023

The dependence of the visible spectrum (harmonics 2 and 3/2) and the output of CuK_α-alpha X-ray radiation on the energy and duration of subrelativistic intensity femtosecond laser pulse acting on a copper foil is investigated. It was found that for secondary radiation, the determining factor is the energy density, and not the intensity and duration of the pulse. The power-law dependencies of the secondary output radiation on the duration and the pulse energy have a significantly different indicator. The tendencies of changing the shape of the spectrum for regions dominated by various mechanisms of plasma heating are revealed.

Keywords: X-ray, second harmonic, harmonic three halves, energy density.

DOI: 10.61011/EOS.2023.02.55781.19-23

Introduction

Ultra-short, spectrally bright pulses of X-ray radiation (XR) are used for diffraction studies with femtosecond time resolution in the pump-probe scheme [1,2], for example, to study forced vibrations of crystal lattice [3], for radiography impact on biological objects [4]. Such pulses can be produced by irradiating solid targets with laser beams of sub-relativistic intensities $I \sim 10^{16}-10^{18}\,\mathrm{W/cm^2}$ [5–8]. The cause of the appearance of characteristic X-ray radiation [6,7] are hot electrons accelerated in the near-surface plasma and returned to the solid part of the target. The near-surface hot plasma is also a source of optical harmonics [8] and other types of secondary radiation. Harmonic generation (SHG — second, THG — three-halves) is of interest not only as a radiation source, but also as a diagnostic tool for processes occurring near the target [9,10].

The spatial area in which the secondary radiation is formed is determined by the concentration of the electrons flying away from the surface n. The reference quantity is the critical electron concentration $n_{\mathrm{cr}} = \omega_0^2 m_e \varepsilon_0 / e^2$, where ω_0— the frequency of laser radiation, ε_0 —vacuum permittivity, m_e, e —mass and charge of electron. When a laser beam ($I \sim 10^{15}-10^{17}\,\mathrm{W/cm^2}$) interacts with a target at an angle of incidence $\theta > 0$ in the area $n = n_{\mathrm{cr}} \cos^2\theta$, the laser pulse is reflected from the target, with closer to the target in the area $n = n_{\mathrm{cr}}$, a mode of resonant absorption of the laser field [11] having penetrated deep into such a plasma occurs, corresponding to the transformation of the longitudinal (along the density gradient) component of the p-polarized electromagnetic wave into longitudinal plasma waves. This regime is accompanied by Langmuir oscillations at the laser frequency and the SHG appearance. In the other area, where the electron concentration is $n = n_{\mathrm{cr}}/4$, a two-plasmon decay process is observed: the laser photon disintegrates into two plasmon with half the frequency. In this case, another laser photon can scatter on such a plasmon with the occurrence of THG [12], indicating electronic plasma instabilities and inhomogeneous extended plasma [10,13]. It is essential that this threshold in intensity and laser pulse duration of the THG process can be related to the „size“ of the plasma L_e and the electron temperature T_e [14].

The predominance of one or another mechanism of energy transfer E from the laser to the plasma is determined in part by its spatial scale of the electron density gradient $L_e = (\frac{1}{N_e}\frac{\partial n}{\partial x})^{-1}$ [15], which can be increased in the experiment by intensity, duration, contrast [5,16] (and thus switch the heating mechanism). With a significant increase in pulse duration τ, the parameter L_e increases at the expense of the plasma dispersion time (characteristic velocity $v_p \sim 0.1-0.2\,\mathrm{nm/fs}$). With contrast (CR) restriction, L_e also increases with the intensity of the incident pulse. According to [16] at $CR = 7 \cdot 10^7$ for $\tau = 30\,\mathrm{fs}$ and intensities $I \sim\ 3 \cdot 10^{16}$, $0.7 \cdot 10^{17}$, $0.7 \cdot 10^{18}\,\mathrm{W/cm^2}$ the characteristic scale is found to be $L_e/\lambda \sim 0.1$, 1, 10, respectively, where λ — is the laser radiation wavelength. For these variation ranges of parameter L_e/λ, the dominant mechanisms of plasma heating in the sub-relativistic case are [17]: vacuum heating [18] at $L_e/\lambda < 0.1$, resonant absorption [11] at $L_e/\lambda \sim 1$ (and in slanted incidence), inverse-bremsstrahlung absorption [17] at $L_e/\lambda \gg 1$. Switching heating mechanisms should affect not only the output of X-rays, but also

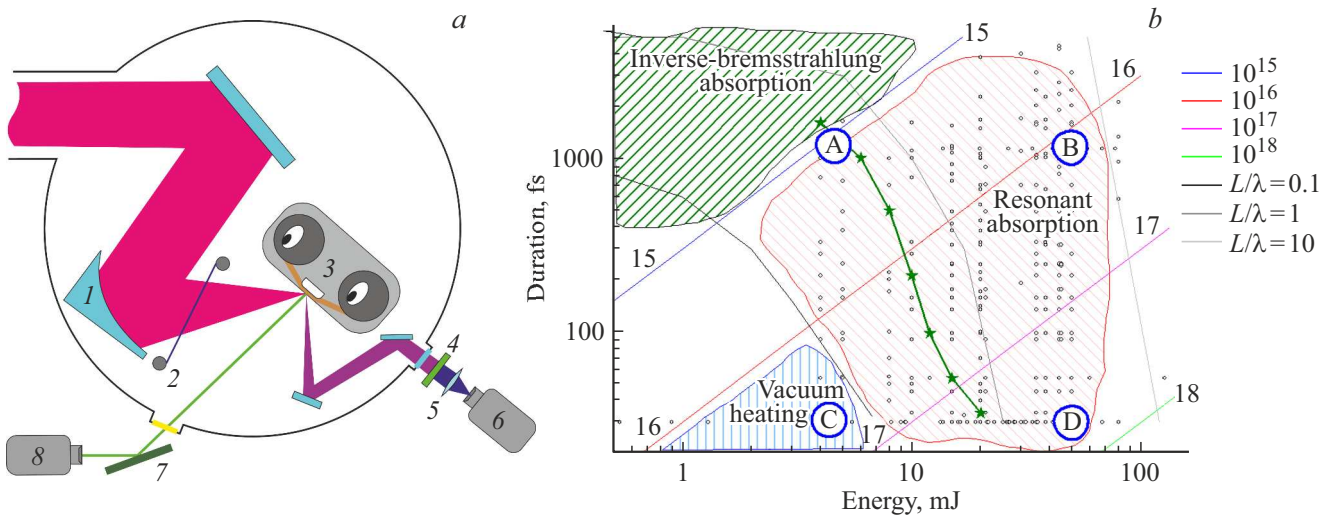

Figure 1. (*a*) Experimental scheme: *1* — off-axis parabola, *2* — protective film, *3* — tape drive with target, *4* - filter, *5* — lens, *6* — spectrometer, *7* — silicon crystal, *8* — PMT. (*b*). Measured points are displayed (black circles) as energy-time field, green asterisks — edge of THG signal appearance. The characteristic points (values E and τ), designated in blue circles as A, B, C, D, are presented as spectra in Fig. 2, *a, b, c, d*, respectively. Inclined straight lines — lines of constant intensity (10^{15}, 10^{16} ... 10^{18} W/cm^2). In areas with different shading, one of the plasma heating processes dominates: inverse-bremsstrahlung absorption (green shading), resonance absorption (red shading), vacuum heating (blue shading). Gray lines — approximate values of $L_e/\lambda = 0.1, 1, 10$ levels for $CR = 10^7$ based on data from [5,16,21].

the harmonic spectra, which are the most quickly and reliably experimentally measured compared to other types of secondary radiation from the target.

From the relative harmonic amplitudes [9,10], we can estimate the actual intensity on the target [1], the radiation contrast [19], and the plasma size [20]. This will allow real-time optimization of the characteristic X-ray emission output and correction of target deviations from the focus.

Therefore, the work has the following aims: 1) establishment of connection of the form of SHG, THG spectra with the intensity on the target and with plasma heating processes, 2) identification of the role of energy and duration of the laser pulse in the generation of secondary radiation (X-ray and optical harmonics) from a femtosecond near-surface laser plasma.

Experiment

The source of the X-ray [6] radiation and harmonics was the plasma generated on the surface of a continuously renewed copper tape 10 μm thick. The tape to be drawn served as a target and was in a vacuum of 10^{-5} mbar. The plasma was generated by oblique (45°) incidence of a *p*-polarized focused TiSa-laser beam from an amplifier system [2,8] with broadband radiation $\lambda = 800 \pm 50$ nm (Fig. 1, *a*). The emission contrast CR was 10^7 (enhanced spontaneous emission) on a time scale of 5 ps and separately 10^5 for the selected femtosecond pre-pulse arriving 10 ns before than the main one. A blue filter (FSB37S, Thorlabs) installed in front of the optical spectrometer attenuates the fundamental frequency of the laser radiation by 4 orders, but still passes it above the noise level in the range up to $\lambda < 830$ nm. This made it possible in a single spectrum measurement to obtain three harmonics at once with their centers at the following wavelengths: SHG — 400 nm, THG — 533 nm, pump — 800 nm, and compare their amplitudes. Bragg diffraction on a silicon ⟨111⟩ [8] crystal was used to extract real-time characteristic CuK_α X-ray radiation from the bremsstrahlung background. The energy of each diffracted pulse (following with a frequency of 10 Hz) was recorded by a photomultiplier equipped with a NaI scintillator. The dependence of secondary emission signals on the energy ($E = 1-120$ mJ) and duration ($\tau = 30-3000$ fs) of laser pulses was studied (Fig. 1, *b*).

The actual diameter of the focal spot on the target was $Ø = 20\,\mu$m, for the maximum energy in this study $E = 120$ mJ, this corresponds to energy density $ED = E/S = 38$ kJ/cm^2 and at $\tau = 30$ fs — intensity $I = E/(S\tau) = 1.2 \cdot 10^{18}$ W/cm^2, where $S = \pi Ø^2/4$ — beam area. Let us compare 4 ultimate cases in duration and energy (marked in Fig. 1, *b*, as A, B, C, D), from the long-weak pulse with $I \sim 10^{15}$ W/cm^2 (case A) to the short-strong one with $I \sim 10^{18}$ W/cm^2 (Case D). All 4 cases are on the edges of the area with the dominance of the resonance absorption process and are adjacent to the areas of other processes. In Case A ($E = 5$ mJ, $\tau = 1000$ fs) we are also close to the area dominated by the inverse-bremsstrahlung absorption mechanism, here, the contribution from collision mechanisms of energy transfer to the plasma is significant. In the other ultimate Case D ($E = 50$ mJ, $\tau = 30$ fs), we approach relativistic heating

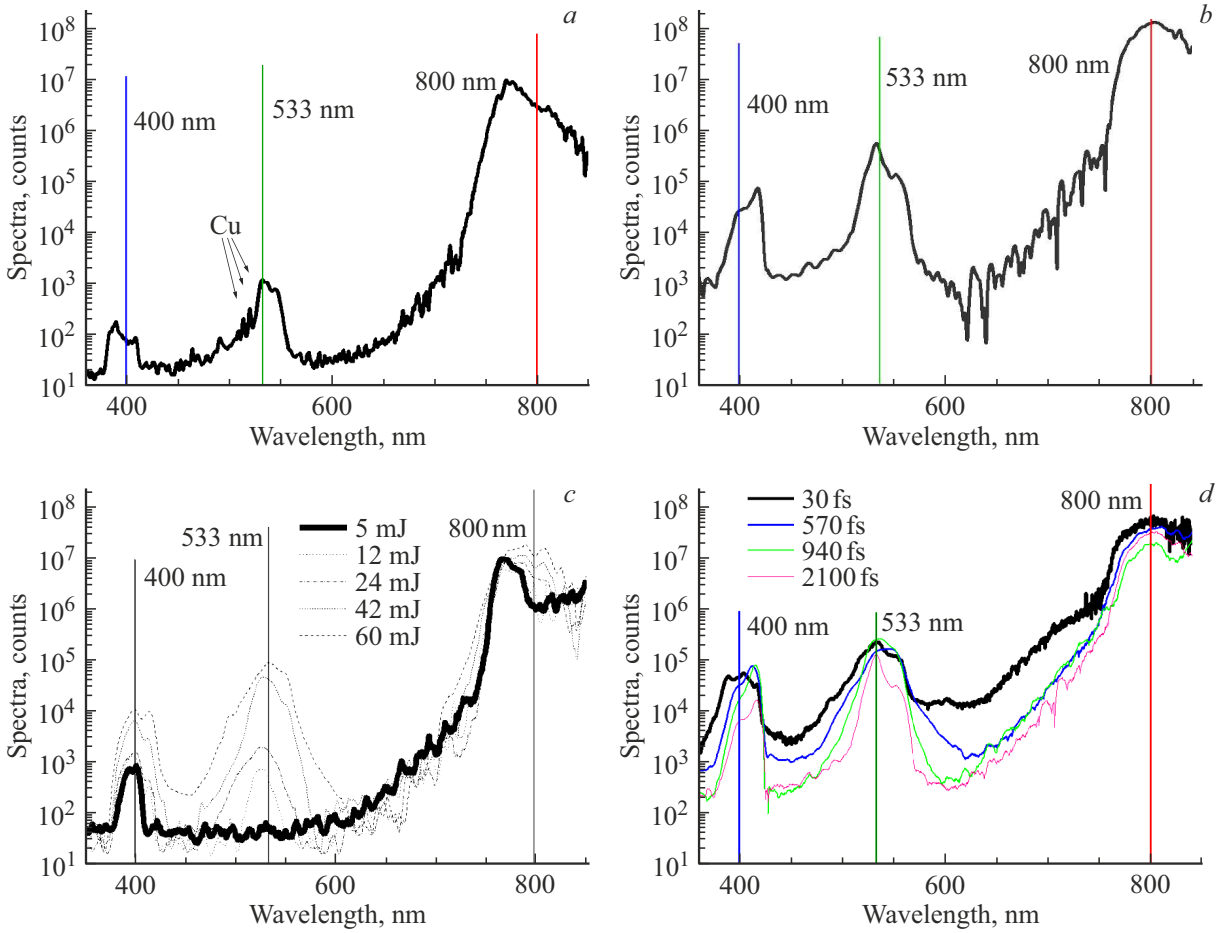

Figure 2. Characteristic spectra in the areas A,B,C,D (black bold curves) marked in Fig. 1, *b*. Accordingly: *a* — long and weak pulse, $I \sim 10^{15}$ W/cm^2, $ED = 1.5$ kJ/cm^2, $\tau = 1000$ fs; *b* — long and strong pulse, $I \sim 2 \cdot 10^{16}$ W/cm^2, $ED = 25$ kJ/cm^2, $\tau = 1000$ fs; *c* — short and weak pulse $\tau = 30$ fs (bold curve at $I \sim 4 \cdot 10^{16}$ W/cm^2, $ED = 1.5$ kJ/cm^2), the dashed lines show changes in the spectrum as the energy increases from 5 to 60 mJ at $\tau = $ const; *d* — short and strong pulse $ED = 25$ kJ/cm^2, the bold black curve at $I \sim 0.8 \cdot 10^{18}$ W/cm^2, the colored curves show the spectrum changes at lower intensities by increasing τ from 30 to 2100 fs with the same E and ED.

mechanisms such as $[j \times B]$ [5,22]. It is assumed that for the long pulse ($\tau > 3000$ fs) the parameter $L_e/\lambda \gg 1$, while for the short pulse ($\tau < 30$ fs, $I < 10^{16}$ W/cm^2) $L_e/\lambda \ll 1$.

Results

At a short pulse and low energy (30 fs, 5 mJ, $ED = 1.5$ kJ/cm^2), no THG is observed (Case C in Fig. 2). The THG threshold is indicated by the green asterisks in Fig. 1, *b*. Note that the THG process is more sensitive than the SHG process to such a pumping parameter as duration.

At $\tau = 1$ ps, THG was observed even for $I = 10^{15}$ W/cm^2 (Case A in Fig. 2). We also note the presence of Cu I atomic copper emission lines at $\lambda = 510, 515, 521$ nm, observed in our measurements only at $I < 10^{15}$ W/cm^2 i. e. at Point A (Fig. 2, *a*), close to the inverse-bremsstrahlung absorption area. As the energy density increases above $ED = 10$ kJ/cm^2, THG appears at any pulse duration, and there is an increase in the ratio with SHG (Fig. 2, *d* and Fig. 3, *a*). At the same time, the spectra of all three harmonics slightly widen, and there is a slight shift to the red band of the SHG and THG peaks (Fig. 2, *c*). As the pulse duration increases, the SHG and THG spectra acquire sharper edges and a lower background (Fig. 2, *d*), and at $\tau > 1$ ps „the top“ of the harmonic spectrum takes on a double-hump shape (Fig. 2, *b, d*). In [19], such a two-humped form of the THG spectrum has been used to determine the temperature of the electrons T_e. In addition, a similar modification of the SHG spectrum was observed in [1]. Note, that Points B and C (Fig. 1, *b*) are almost at the same intensity $\sim 3 \cdot 10^{16}$ W/cm^2, but differ by an order of magnitude in energy density (1.5 and 25 kJ/cm^2). At the same time, the secondary emission signals in Case B are 1–2 order stronger than in Case C (Fig. 2, *b, c*), which emphasizes the importance of the ED parameter, but not I.

As the measured quantity Y_j ($j =$ SHG, THG, pump, XR) is the energy of the corresponding pulse, for the

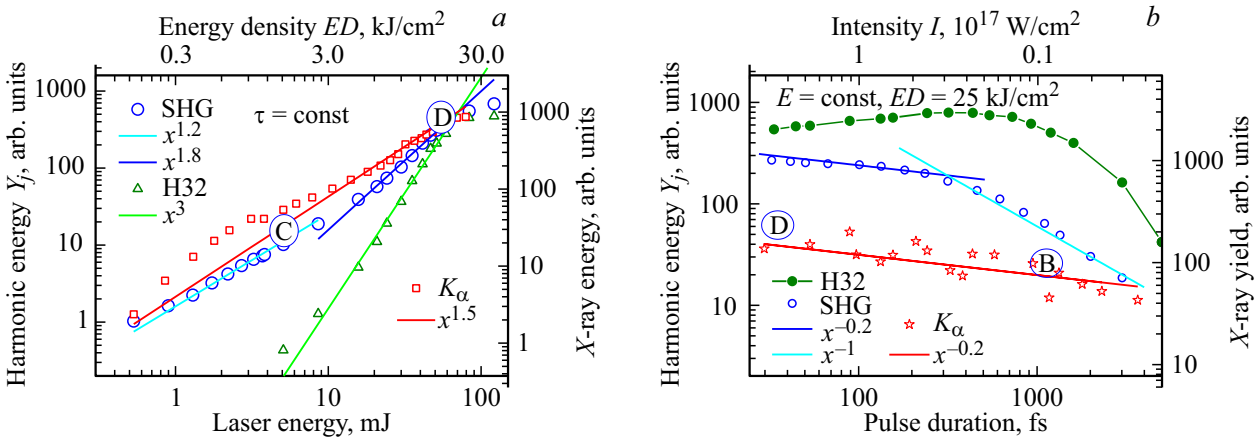

Figure 3. Energy dependence of harmonics Y_{SHG} (SHG), Y_{THG} (H32) and XR (K_α) on (a) energy (and synchronously changing energy density at a fixed laser pulse duration of 30 fs); (b) from the laser pulse duration (and synchronously varying intensity at a fixed pumping energy 50 mJ). Points B, C, D are the attachments to the corresponding areas in Fig. 1, b.

harmonics case, it is the integral of the spectrum over wavelengths 370–430 nm for SHG, 480–620 nm for THG, 750–830 nm for pump. The integration range is chosen „with a margin of “, but so as not to visually overlap with the neighboring harmonic. The change in SHG magnitude during energy and duration scanning can be represented as $Y_{SHG} \sim E^{(1.6\pm0.2)}/\tau^{0.2}$. The change in the exponent from 1.2 to 1.8 around $E = 8$–10 mJ, $\tau = 30$ fs observed in Fig. 3, a) just corresponds to a change in the mechanism of vacuum heating to resonance absorption (Fig. 1, b) by increasing L_e/λ with increasing energy and intensity.

In case of THG, the amplitude change is proportional to $Y_{THG} \sim E^{(3\pm0.2)}/f(\tau)$, and the dependence on $f(\tau)$ is non-monotone (Fig. 3, b). Pump (as long as the intensity is below relativistic) depends linearly on E and does not depend on τ: $Y_{pump} \sim E$. From the ratio of harmonic amplitudes in practice, it is convenient to determine the actual energy density on the target (for a fixed angle of incidence, contrast and τ). Under the conditions of this experiment $ED \sim (15\,\text{kJ/cm}^2)(Y_{THG}/Y_{SHG})^{0.7}$, and also $ED \sim (4 \cdot 10^6\,\text{kJ/cm}^2)(Y_{SHG}/Y_{pump})^{1.6}$. Note, that when the incidence angle on the target was decreased from 45° to 15° by about 5 times, the ratio Y_{THG}/Y_{SHG} the X-ray yield for most energies and durations used also decreased, confirming the predominance of the resonance absorption. The qualitatively described above trends of changes in the spectra were preserved, including for the plastic target.

As for XR, as for harmonics, the output of Y_{XR} increases with increasing laser pulse intensity at different „rates“ (degrees), depending on the way the intensity is increased. When the intensity increases due to growth E (and accordingly ED when $\tau = \text{const}$, Fig. 3, a) $Y_{XR} \sim x^{1.5}$, but when the intensity is increased by shortening the duration, when $E = \text{const}$, Fig. 3, b) $Y_{XR} \sim x^{0.2}$. The output K_α can be described as $Y_{K\alpha} \sim E^{1.5\pm0.2}/\tau^{0.2}$. At practice-optimal parameters found ($\tau = 200$–300 fs, $E = 50$–80 mJ, $ED = 15\,\text{kJ/cm}^2$, $I = 10^{17}\,\text{W/cm}^2$), the yield of characteristic X-ray photons $5 \cdot 10^8$ photon/pulse·2π is sufficient for applications, and high-energy bremsstrahlung X-ray photons and accelerated electrons do not cause appreciable noise to detectors. These conditions (requirement of focus, optimal duration) are found by the ratio of harmonic energies $Y_{SHG}/Y_{THG} \sim 1$ and $Y_{pump}/Y_{SHG} \sim 10^3$.

Conclusions

The yield of secondary radiation from a femtosecond laser plasma (characteristic XR, visible range harmonics) is determined primarily by the energy density rather than the intensity or duration of the pump pulse. Increasing the duration of femtosecond laser pulses from 30 to 300 fs practically does not attenuate the output of secondary radiation in the intensity range from 10^{15} to $10^{18}\,\text{W/cm}^2$.

For $\tau = 30$ fs, THG appears at $ED > 2.5\,\text{kJ/cm}^2$, is compared in amplitude with SHG at $ED \sim 25\,\text{kJ/cm}^2$, slightly exceeds SHG with further increase in pump energy. Significant dominance of THG over SHG occurs for pulses with durations greater than 300 fs. Spectral splitting of the SHG and THG peaks indicates a picosecond pulse duration. The broadening and overlapping of the wings of the harmonic spectra indicate an approach to relativistic intensity, most noticeable is the broadening of the pump into the blue band at $10^{18}\,\text{W/cm}^2$.

The differences in conversion between the different modes (resonant absorption, vacuum heating) are reduced to a change in the power density dependence index by $\sim \pm0.2$. The characteristic scale L_e/λ affects the shape of the optical spectra, the position of the kinks of the power dependences of the harmonic energies $Y_j(E, \tau)$ and requires more systematic investigation for a number of incidence angles and contrasts.

Funding

This study was supported in part by the Russian Ministry of Science and Higher Education of the Russian Federation under Agreement № 075-15-2022-830, dated May 27, 2022, and RFBR grants 20-21-00140 and 19-29-12037 mk.

Conflict of interest

The authors declare that they have no conflict of interest.

References

[1] D. von der Linde, H. Schulz, T. Engers, H. Schuler. IEEE J. Quant. Electron., **28** (10), 2388 (1992). DOI: 10.1109/3.159545

[2] M.V. Kovalchuk, M.M. Borisov, A.A. Garmatina, V.M. Gordienko, A.M. Zheltikov, V.V. Kvardakov, V.N. Korchuganov, I.A. Likhachev, E.I. Mareev, A.V. Mitrofanov, M.M. Nazarov, E.M. Pashaev, F.V. Potemkin, Ya.O. Romanovskii, E.B. Rudneva, D.A. Sidorov-Biryukov, I.A. Subbotin, M.V. Chashchin, P.A. Shcheglov, V.Ya. Panchenko. Crystallography Reports, **67** (5), 717 (2022). DOI: 10.1134/S106377452205008X.

[3] M. Nicoul, U. Shymanovich, A. Tarasevitch, D. von der Linde, K. Sokolowski-Tinten. Appl. Phys. Lett., **98** (19), 191902 (2011). DOI: 10.1063/1.3584864

[4] M. Nishikino, K. Sato, N. Hasegawa, M. Ishino, S. Ohshima, Y. Okano, T. Kawachi, H. Numasaki, T. Teshima, H. Nishimura. Rev. Sci. Instruments, **81** (2), 026107 (2010). DOI: 10.1063/1.3302827

[5] M.V. Sedov. *Modelirovanie kharakteristicheskogo rentgenovskogo izlucheniya femtosekundnoy lazernoy plazmy*. (In Russian) Synopsis of PhD thesis. (St. Petersburg State University, St. Petersburg, 2019).

[6] V. Arora, P.A. Naik, J.A. Chakera, S. Bagchi, M. Tayyab, P.D. Gupta. AIP Adv., **4** (4), 047106 (2014). DOI: 10.1063/1.4870946

[7] R. Rathore, V. Arora, H. Singhal, T. Mandal, J.A. Chakera, P.A. Naik. Laser and Particle Beams, **35** (3), 442 (2017). DOI: 10.1017/S026303461700043X

[8] M.M. Nazarov, P.A. Shcheglov, A.A. Garmatina, M.V. Chashchin, Z.C. Margushev, K.A. Bzheumikhov, A.V. Mitrofanov, D.A. Sidorov-Biryukov, A.M. Zheltikov, V.M. Gordienko, V.Ya. Panchenko. Kvant. elektron., **52** (9), 811 (2022) (in Russian).

[9] K.A. Ivanov, I.N. Tsymbalov, S.A. Shulyapov, D.A. Krestovskikh, A.V. Brantov, V.Yu. Bychenkov, R.V. Volkov, A.B. Savel'ev. Phys Plasmas, **24** (6), 063109 (2017). DOI: 10.1063/1.4986101

[10] P.K. Singh, A. Adak, A.D. Lad, G. Chatterjee, G.R. Kumar. Phys Plasmas, **27** (8), 083105 (2020). DOI: 10.1063/5.0012590

[11] D.W. Forslund, J.M. Kindel, K. Lee, E.L. Lindman, R.L. Morse. Phys. Rev. A (Coll Park), **11** (2), 679 (1975). DOI: 10.1103/PhysRevA.11.679

[12] L. Veisz, W. Theobald, T. Feurer, H. Schillinger, P. Gibbon, R. Sauerbrey, M.S. Jovanović. Phys Plasmas, **9** (8), 3197 (2002). DOI: 10.1063/1.1493794

[13] I.N. Tsymbalov, D.A. Gorlova, V.Yu. Bychenkov, A.B. Savel'ev. Quantum Electronics, **49** (4), 386 (2019). DOI: 10.1070/QEL16941.

[14] T.J.M. Boyd. Plasma Phys Control Fusion, **28** (12B), 1887 (1986). DOI: 10.1088/0741-3335/28/12B/002

[15] P. Gibbon, E. Förster. Plasma Phys Control Fusion, **38** (6), 769 (1996). DOI: 10.1088/0741-3335/38/6/001

[16] M. Gambari, R. Clady, L. Videau, O. Utéza, A. Ferré, M. Sentis. Sci. Rep., **11** (1), 23318 (2021). DOI: 10.1038/s41598-021-02585-5

[17] P. Gibbon. *Short Pulse Laser Interactions with Matter: An Introduction*, 1st ed. (Imperial College Press, 2005). DOI: 10.1142/p116

[18] F. Brunel. Phys. Rev. Lett., **59** (1), 52 (1987). DOI: 10.1103/PhysRevLett.59.52

[19] P.K. Singh, A. Adak, A.D. Lad, G. Chatterjee, P. Brijesh, G. Ravindra Kumar. Phys. Plasmas, **22** (11), 113114 (2015). DOI: 10.1063/1.4935909

[20] C. Li, M.-L.L. Zhou, W.-J.J. Ding, F. Du, F. Liu, Y.-T.T. Li, W.-M.M. Wang, Z.-M.M. Sheng, J.-L.L. Ma, L.-M.M. Chen, X. Lu, Q.-L.L. Dong, Z.-H.H. Wang, Z. Lou, S.-C.C. Shi, Z.-Y.Y. Wei, J. Zhang. Phys. Rev. E, **84** (3), 036405 (2011). DOI: 10.1103/PhysRevE.84.036405

[21] L.M. Chen, M. Kando, M.H. Xu, Y.T. Li, J. Koga, M. Chen, H. Xu, X.H. Yuan, Q.L. Dong, Z.M. Sheng, S.V. Bulanov, Y. Kato, J. Zhang, T. Tajima. Phys. Rev. Lett., **100** (4), 045004 (2008). DOI: 10.1103/PhysRevLett.100.045004

[22] W.L. Kruer, K. Estabrook. Physics of Fluids, **28** (1), 430 (1985). DOI: 10.1063/1.865171

Translated by Y.Deineka